ACS OMEGA

Open Access



http://pubs.acs.org/journal/acsodf

Article

# Molecular Evidence of Structural Changes in Silk Using Unlimited Degradation Mass Spectrometry

Jie Zhou, Xiong Zhou, Lindan Pan, Yefeng Deng, Hailing Zheng, Zhiqin Peng, Junmin Wan, Yang Zhou, and Bing Wang*

Cite This: *ACS Omega* 2023, 8, 34410−34419

Read Online

ACCESS | Metrics & More | Article Recommendations | Supporting Information

**ABSTRACT:** Proteomics has important uses in archeological science because it can distinguish species, reveal the evolution of paleontology, and provide biological evidence of historical events. However, this technique still has full potential in the study of silk aging mechanisms. In this work, we propose a strategy combining unlimited degradation with mass-spectrometry-based proteomics techniques, which interpret protein fragmentation propensity and secondary structure changes by detecting content changes of specific peptide groups in complex proteomes. This approach was employed to study the conformational changes in silk microscopic crystals after heat treatment. Combining conventional mechanics and crystallographic characterization, a thermal aging degradation mechanism model was proposed. At the same time, it explained the interesting problem that the crystallinity remained unchanged, but the mechanical properties decreased significantly. Focusing on the unlimited degradation process, this method will be widely applicable to the study of silk and wool aging processes and regenerated silk fibroin.

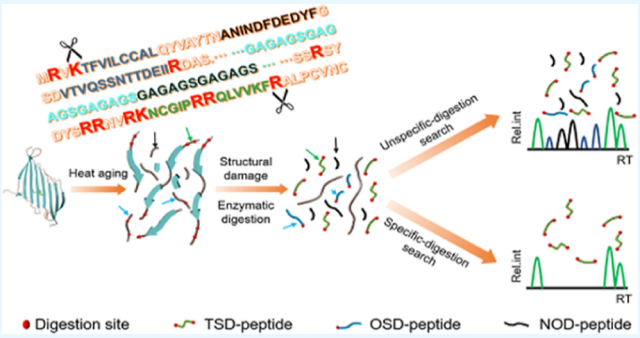


## INTRODUCTION

Silk, a biopolymer constituted by a variety of proteins,[1] was broadly applied in ancient textile production. The first use of silk to produce textiles was estimated to have occurred in the Yang Shao culture period more than 5000 years ago. Unfortunately, direct evidence of this is lacking due to physical and chemical factors[2−5] involving microorganisms, temperature, pH, force, and so on. Silk degradation made it very difficult to trace its existence, let alone its origin. The protection of silk is also very difficult. Thus, it is imperative to discover an accurate silk degradation mechanism that would facilitate the proposal of new ideas for microscopic trace detection and cultural relic protection. Furthermore, silk has been repurposed in new material engineering, especially for biomedical applications.[6,7] The monitorable and controlled degradation processes of silk fibroin are key to obtaining target materials. Thus, understanding degradation mechanisms could also contribute to the development of improved silk-based materials.

Research on silk degradation has been frequently conducted in recent years. Biodegradation and physicochemical degradation are usually simulated by accelerated-aging methods. For example, exposing silk to various protease solutions was thought to simulate the microbial aging process,[8] and alkaline solutions were selected to simulate alkaline soils and alkaline secretions.[9] All of these processes were monitored by a variety of characterization methods. Thus, it is critical to be able to monitor the changes in the structure of silk fabrics.

Degummed *Bombyx mori* (*B. mori*) silk, a semicrystalline protein polymer with high tensile strength and toughness,[10] was used in the weaving of historic silk fabrics. Silk fibroin is mainly composed of heavy chain (350 kDa), light chain (26 kDa), and integrity-maintaining glycoprotein p25 (30 kDa) in a molar ratio of 6:6:1.[11,12] The heavy chain and light chain are linked by disulfide bonds at their C-termini.[13] The heavy chain sequence contains a regular repetition of $(GAGAGS)_n$ segments, which served as the main fragment that makes up the crystalline region.[14,15] Takahashi et al.[16] adopted a repeating unit of $(Gx)_n$ as the first approximation of their structural models. These repetitive $(GAGAGS)_n$ segments are widely distributed in 12 GX-repeat encoding regions isolated by 11 similar randomly intervening sequence-encoding regions. For *B. mori* silk fabrics, these $\beta$-sheet structures composed of continuous $(GAGAGS)_n$ segments are a central factor in their high performance.[10,17]

Fourier transform infrared (FTIR) spectroscopy,[18] Raman spectroscopy,[19] and X-ray crystallography[20] were performed to analyze the changes in protein structure, especially those regarding crystal structure. However, the corresponding results

**Received:** April 4, 2023
**Accepted:** August 3, 2023
**Published:** September 16, 2023

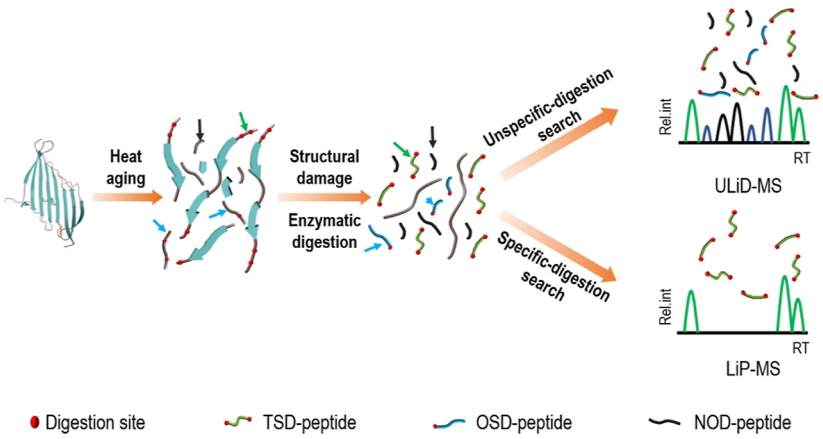


**Figure 1.** ULiD-MS workflow. In the first step, a proteome extracted from silk fabrics is subjected to double digestion. The first digestion is conducted using heat aging, which will replace broad-specificity protease. Next, a LiP trypsin (the C-terminus of K and R) digestion generates peptides suitable for bottom-up MS analysis. The peptide mixture includes two side digestion peptide groups (TSD-peptide), one side digestion peptide group (OSD-peptide), and no digestion peptide group (NOD-peptide). Subsequently, the samples are subjected to limited and/or unlimited mass-spectrometry analyses (LiP-MS and ULiD-MS).

were insufficient to demonstrate a degradation mechanism due to a lack of structural analysis at the molecular level. The proteomics technique, which has become an efficient and accurate new approach for the identification and deterioration mechanism research of cultural objects,[21,22] was used to detect the amino acid sequence, species, and abundance of proteins. However, the identification of protein structural transitions could also be performed by proteomics.[23] Feng et al.[24] presented a method that coupled limited proteolysis (LiP) with a targeted proteomics workflow, which enabled the monitoring of structural changes in proteins on a large scale. Owing to the special characteristics of silk proteins, nonspecific proteases have difficulty performing enzymatic digestion without damaging protein structures, and the global analysis of protein structural changes cannot achieve the desired effect.

In this work, a novel unlimited degradation mass spectrometry (ULiD-MS) approach was developed for probing the structural transitions of silk after heat treatment, including the changes in protein and peptide components (Figure 1). To understand the heat-aging degradation mechanism, SEM, tensile tests, FTIR, XRD, and sodium dodecyl sulfate−polyacrylamide gel electrophoresis (SDS−PAGE) analyses were also used to study the morphology, mechanical property, secondary structure, and molecular weight distribution. This work can provide molecular-level evidence for the degradation behavior of silk.

## EXPERIMENTAL SECTION

**Reagents.** Ethanol, calcium chloride, sodium dodecyl sulfate (SDS), bromophenol blue, tris(hydroxymethyl)-aminomethane hydrochloride (Tris-HCl) and tris(hydroxymethyl)-aminomethane were provided by Alad-din. A protease inhibitor cocktail and phosphorylase inhibitor were supplied by Merck Millipore. Iodoacetamide (IAM) and urea were purchased from Sigma-Aldrich (Aladdin). The silk fabrics were provided by Hang-zhou Fusi Industry and Trade Co., Ltd. The water used in all experiments was purified with a TPM Ultrapure water system.

**Heating Conditions.** A heating treatment was applied to obtain artificially heat-aged samples. The silk fabric (SF) was cut into strips of 2 cm × 20 cm, keeping the sample length and width in line with the silk's warp and weft. After washing, drying, and weighing, the silk fabric strips were suspended in an HW-450AS far-infrared drying oven at 140 °C for 0, 2, 4, 6, 8, and 10 d. Each sample (SF-0 d, SF-2 d, SF-4 d, SF-6 d, SF-8 d, and SF-10 d) was weighed immediately after being taken from the oven.

**Morphological Characterization and Mechanical Test.** After washing and drying, the morphological characterization of the SF samples was performed using scanning electron microscopy (SEM) (JSM 5610LV: Shimadzu Co., Japan). Then, all silk fabric strips were secured to the clamps of stretching cells between a force sensor and the stage. With an effective stretch length of 5 cm, the strips were deformed through tension at a constant extension rate (2 mm/min). For the stress calculations, the cross-sectional area was approximated by a rectangle, whose height was determined by Vernier calipers. Three samples were tested at each sampling time. The stress−strain curves closest to the average were chosen. The Young's modulus and elongation at break were derived from an average of three stress−strain curves for each sampling time.

**FTIR and XRD.** The FTIR spectrum was acquired using a Fourier infrared spectrum instrument (Nicolet 5700: PerkinElmer Company, USA) in the range between 400 and 4000 $cm^{-1}$ with a spectral resolution of 1 cm. The data to determine the protein numbers and positions were obtained from second-derivative spectra and deconvolved. Then, the height, bandwidth position, and baseline were iteratively adjusted to obtain the best Gauss/Lorentzian shaped curve, and the amide I region spectrum was resolved into individual secondary structural components. After fitting the distinguishing peak of amide I, we obtained the band area of each group and used it to calculate the relative proportion of the components in the secondary structure. The degree of crystallinity of the artificially heat-aged samples was evaluated by wide-angle X-ray diffraction (WAXD) analysis using an X-ray diffractometer (Thermo ARL, Switzerland). All peak separation processes were implemented via Origin 2018. The degree of crystallinity ($X_c$) was estimated as previously reported[25] using the following formula: $X_c = I_c/(I_c + I_a) \times 100\%$, where $I_c$ and $I_a$ are the total intensities of the crystalline and amorphous diffraction peaks, respectively.

**Extraction of Silk Fibroin.** After removing both ends, 50 mg of silk fabric was dissolved in 5 mL of $CaCl_2$−$C_2H_5OH$−$H_2O$ (molar ratio of 1:2:8) solution under shaking at 96 °C for 1 h. According to previous reports,[9,26] all the protein components in silk fabrics can be completely dissolved. The solution was then


https://doi.org/10.1021/acsomega.3c02254
ACS Omega 2023, 8, 34410−34419

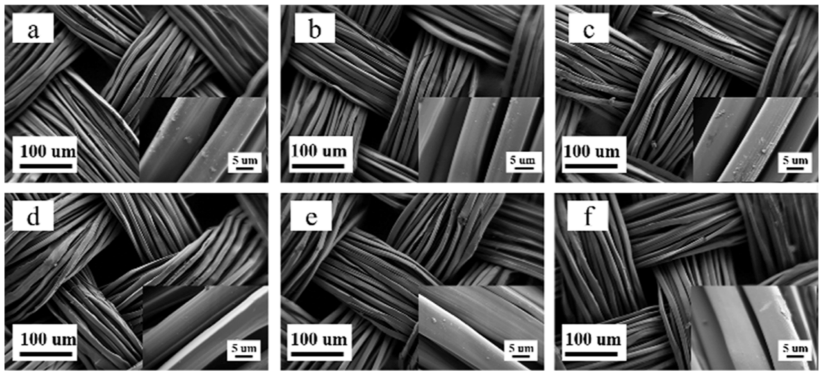


**Figure 2.** SEM of silk fabrics after the thermal aging test: (a) SF-0d, (b) SF-2d, (c) SF-4d, (d) SF-6d, (e) SF-8d, and (f) SF-10d. Inset is the local magnification of the sample.

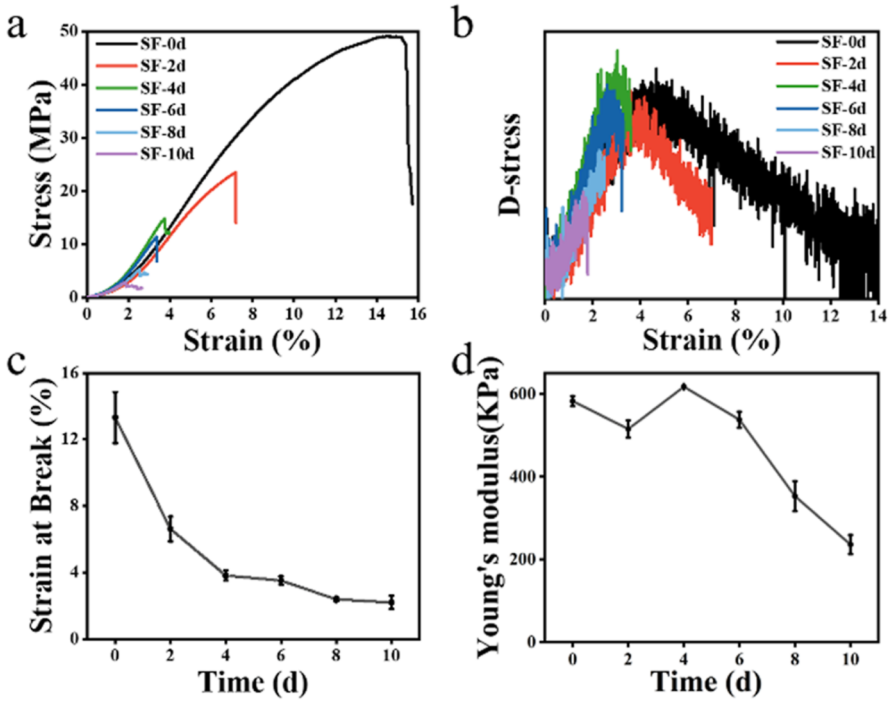


**Figure 3.** (a) Stress−strain curves of silk fabrics after thermal aging test. (b) Derivative diagram of stress−strain curve. (c) Evolution of the elongation at break after heat treatment. (d) Evolution of the Young's modulus at break after heat treatment.

dialyzed (MWCO 1000 Da) against deionized water for 72 h and lyophilized for 24 h. The dried silk fibroins were stored at −20 °C for further experiments.

**Sodium Dodecyl Sulfate−polyacrylamide Gel Electrophoresis (SDS−PAGE).** Approximately 10 mg of silk fibroin was dissolved in 1 mL of carbonate buffer (CB, pH 9.6) mixed with 250 μL of loading buffer (0.5 M Tris-HCl, 0.8% DTT, and 1% SDS). After being boiled for 10 min, the solution was loaded in a gel swim lane in electrophoresis buffer (0.025 M Tris, 0.25 M glycine, 0.1% SDS) for 1 h. The detailed SDS−PAGE procedures were reported in our previous study.[27]

**Protein Digestion and LC−MS/MS.** The dried silk fibroins were dispersed in lysis buffer (1% SDS, 1% protease inhibitor cocktail) and sonicated on an ice bath. An equal volume of protein (concentrations of the silk fibroins were measured by a BCA assay) was reduced with 5 mM dithiothreitol for 30 min at 56 °C and then alkylated with 11 mM iodoacetamide for 15 min at room temperature in darkness. After the protein sample was diluted by adding 100 mM TEAB to attain a urea concentration of less than 2 M, sequencing-grade modified trypsin was added at a 1:50 trypsin-to-protein mass ratio for the first digestion overnight and a 1:100 trypsin-to-protein mass ratio for a second 4 h digestion. The peptides were desalted with a C18 SPE column. The tryptic peptides were dissolved in solvent A (0.1% formic acid, 2% acetonitrile/in water) and directly loaded onto a custom-built reversed-phase analytical column (25 cm length, 75 μm i.d.). Peptides were separated with a gradient of 5 to 25% solvent B (0.1% formic acid in 90% acetonitrile) over 60 min, 25 to 35% in 22 min, reaching 80% in 4 min, and then holding at 80% for the last 4 min, all at a constant flow rate of 450 nL/min using an EASY-nLC 1200 UPLC system (Thermo Fisher Scientific).

The separated peptides were analyzed using a Q Exactive HF-X instrument (Thermo Fisher Scientific) with a nano-electrospray ion source. The applied electrospray voltage was 1.5 kV. The peptide parent ions and their secondary fragments were detected and analyzed using high-resolution TOF. The full MS scan resolution was set to 60,000 for a scan range of 100−


https://doi.org/10.1021/acsomega.3c02254
ACS Omega 2023, 8, 34410−34419

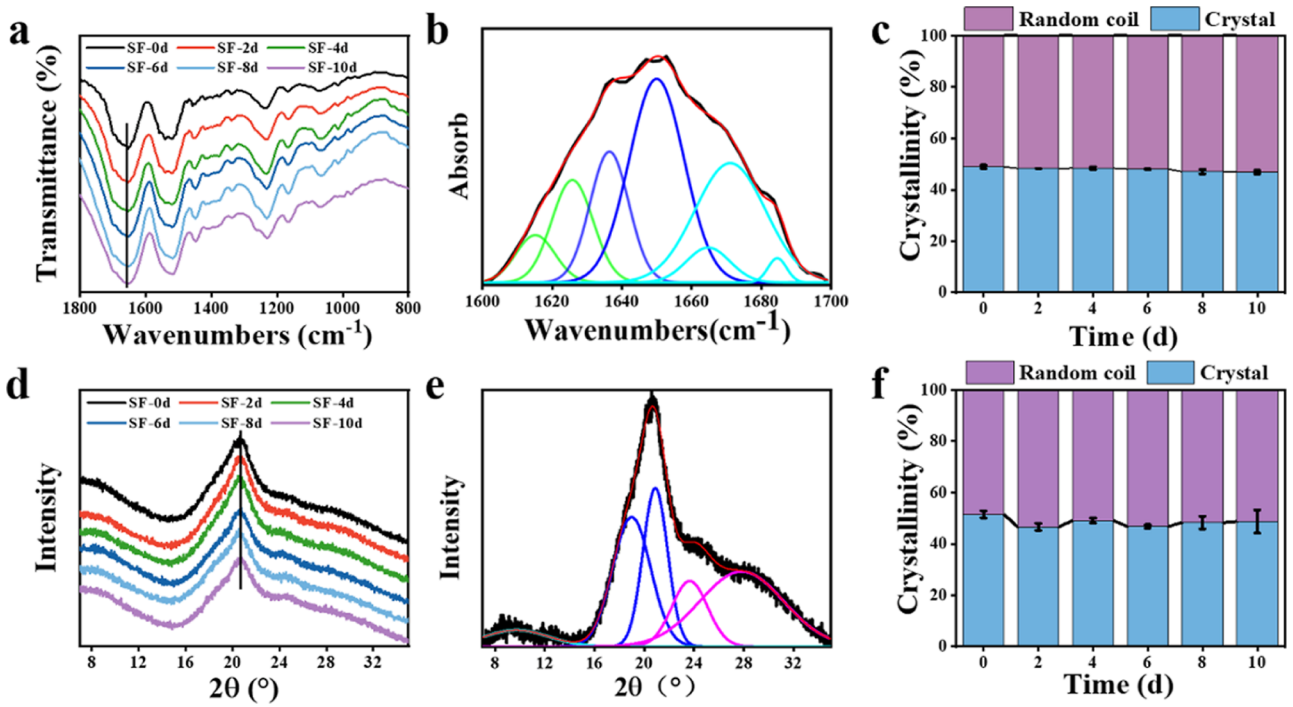


**Figure 4.** Crystallographic assay of thermal aging fabrics. (a) FTIR spectra of silk fabrics after thermal aging. (b) Results of FTIR peak separation analysis. (c) Crystallinity change with the increasing heat treatment time obtained from FTIR analyses. (d) XRD spectra of silk fabrics after the thermal aging test. (e) Results of XRD peak separation analysis. (f) Crystallinity change with the increasing heat treatment time obtained from XRD analyses.

1700 $m/z$. The 20 most abundant precursors were then selected for further MS/MS analyses with a 30 s dynamic exclusion. HCD fragmentation was performed at a normalized collision energy of 28%. The fragments were detected using an Orbitrap at a resolution of 30,000. The fixed first mass was set as 100 $m/z$. The automatic gain control target was set at 1E5, with an intensity threshold of 3.3 E4 and a maximum injection time of 30 ms.

**Identification and Quantification of Proteins and Peptides.** The collected spectra were searched against the Blast_Bombyx_mori_7091_PR_20220314.fasta [14,777 proteins from UniProt-Proteome UP000005204-Bombyx mori (Silk moth)] protein database with Maxquant (v2.0.3.0). The Decoy database was added to calculate the false positive rate (FDR) due to random matches, and a common contaminating database was added to remove the effects of contaminating proteins from the identification results. The digesting protease was set as trypsin with a tolerance of two missed cleavages. The minimum peptide length was set to seven amino acid residues, with a maximum number of five peptide modifications. The mass error tolerance for the primary parent ion was set to 20 ppm for the first search and 20 ppm for the main search, and that for the secondary fragment ion was set to 20 ppm. Carbamidomethyl (C) was defined as a fixed modification, and oxidation (M) and acetyl (protein N-tern) were defined as variable modifications. The FDR for protein identification and PSM identification was set to 1%. Then, these parameters were used to analyze the data to obtain LiP-MS data.

To compare and analyze the degradation of the protein due to heat degradation, unlimited degradation mass spectrometry (ULiD-MS) data were acquired by using the new appropriate analysis parameters. The same collected spectra were submitted to Bombyx_mori_7091_3protein_20220507.fasta (P05790, P04148, and P21828 from UniProt), and nonspecific digestion was set as the digesting protease. Then, they were used for a database search with the parameters described above. All identified proteins and quantified peptides were provided in Supporting Information.

## RESULTS AND DISCUSSION

**Morphology and Mechanical Properties of Heat-Aged Silk Fabrics.** The surface morphologies of the heat-aged samples are listed in Figure 2. Although a small amount of lateral cracking was found on the surface of the heat-aged silks, this phenomenon also occurred in blank control and did not worsen with prolonged heat treatment. In addition, all magnified SEM images (inset) showed pronounced silk characteristics with a smooth surface and vertical lines, suggesting heat treatment would not cause morphological defects.

On the contrary, after heat treatment at 140 °C, the mechanical properties of the silk fabrics were greatly changed. As shown in Figure 3a, the mechanical properties of the heat-aged samples were reduced compared to those of the blank samples. A more detailed analysis of the mechanical parameters is shown in Figure 3b−d. The elongation-at-break and strength, which changed from 15 to 1.8% (Figure 3c), of the samples decreased significantly with the time of heat treatment. The decrease in the elongation-at-break for heat-aged samples was reflected on the molecular scale by the degradation of fibroin. The derivative of the stress−strain curve represents the instantaneous Young's modulus variation trend of the fabric (Figure 3b). The peak for SF-0 that appeared at a tensile strain of 4% was attributed to the deformation of the $\beta$-sheet structures. All stress−strain derivative diagrams showed a high degree of consistency for the samples before fracture. The Young's modulus of all samples with a tensile strain greater than 4% fluctuated between 500 and 600 kPa and showed no significant difference (Figure 3d).


https://doi.org/10.1021/acsomega.3c02254
ACS Omega 2023, 8, 34410−34419

**Secondary Structure of Heat-Aged Silk Fabrics.** Silk is a typical protein fiber that has three characteristic regions, amide I (1700−1600 $cm^{-1}$), amide II (1600−1500 $cm^{-1}$) and amide III (1300−1180 $cm^{-1}$), in its FTIR spectrum. The amide I band is highly sensitive to small variations in molecular geometry and hydrogen bonding patterns, and each type of secondary structure gives rise to a different C═O stretching frequency.[28] It is therefore especially useful for the analysis of the secondary structure composition and conformational changes of proteins. According to previous reports,[29−31] the bands between 1700 and 1656 $cm^{-1}$ are attributed to proteins with $\alpha$-helical components. The bands between 1634 and 1600 $cm^{-1}$ are attributed to $\beta$-sheet structures. The peak that represents the random coil conformation is located at 1655−1635 $cm^{-1}$. After fitting the peak of amide I for each group of samples, the average ratios of the $\alpha$-helix and $\beta$-sheet structures of the three samples were calculated to obtain the crystallinity changes of the heat-aged samples. As shown in Figure 4a−c, the main peak of amide I for silk was located at 1648 $cm^{-1}$. No bathochromic shift occurred for any of the samples. Then, the seven Gauss-Lorentzian peak areas separated by the amide I region were calculated (Figures 4b and S2). The degrees of crystallinity of the silks only showed a slight decrease trend with the prolongation of heat treatment, and all of them were close to that of the blank sample.

The changes in the crystallinity of silk were further characterized by XRD. The peaks in the XRD patterns located at 9.1, 12.2, 18.9, 19.7, 20.7, 24.3, and 24.7° were attributed to the crystalline regions of silk.[19,32] The sharp characteristic diffraction peak at 20.7° was highly consistent for all samples (Figure 4d), which confirmed the high similarity of the amide I regions in the FTIR spectra. The intensities of the crystalline and amorphous peaks evaluated by peak separation analysis were used to calculate the crystallinity (Figures 4e and S3). The crystallinity change results are shown in Figure 4f. There was little variation between the duplicate samples, and heat treatment had an even smaller effect on the sample crystallinity than the replicate variation, which was consistent with the FTIR results. The mutual confirmation of these two characterization methods showed that thermal aging did not affect the crystallinity of silk fibroin.

**Molecular Weight Distribution of Heat-Aged Silk Fabrics.** SDS−PAGE revealed the lengths of the peptides present in the sample. As shown in Figure 5, there were diffuse bands above 15 kDa for all samples, which meant that peptide breakage occurred in all samples. The blank sample showed a wide band between 15 and 250 kDa, especially between 30 and 150 kDa, which primarily indicated the breakage of the fibroin heavy chain. The artificially aged samples displayed a negative

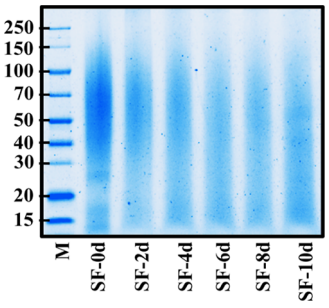


**Figure 5.** SDS−PAGE of silk fabrics after thermal aging.

correlation of $M_r$ with aging time. After 8 days of heat-aging, the $M_r$ of samples was mainly distributed at 15−50 kDa, i.e., long peptides were greatly reduced while short peptides were increased, also suggesting the increase of the degradation degree. Silk fibroin is a molecular complex composed of a heavy chain (350 kDa), a light chain (26 kDa), and a P25 chain (30 kDa) connected via disulfide bonds and noncovalent forces.[9,12] Most of the peptides in the crystallized regions were greater than 30 kDa. Thus, the disappearance of peptides above 30 kDa may indicate degradation in the crystalline region, which was later confirmed.

**Identification and Relative Abundance of Proteins in Silk.** Bottom-up proteomics is based on the measurement of peptides derived from protein digestion, which means that the identified peptides must be reassigned to their maternal proteins.[33] The determination of protein intensity can reflect the integrity of the amino acid sequence of an identified protein. However, due to the specificity of the enzyme, only the sequence of the specific region containing the cleavage site (enzymatic digestion region) can be detected. As shown in the partially intercepted heavy chain sequence digested by trypsin (Figure 6c), only 3% of the heavy chain contains cleavage sites, which contain only small amounts of K and R amino acids at both ends of the heavy chain. All the GX-repeats belong to the nonenzymatic digestion region. As shown in Figure 6a,b, the peptide coverage of LiP-MS indicated that the region specifically cleaved by trypsin is only a small part of the whole. The peptide coverage of the fibroin heavy chain (P05790) increased from approximately 3% (Figure 6a) to 70% (Figure 6b). For the light chain and p25 chain, although the cleavage sites are evenly distributed in their protein sequences, the peptide coverage of the light chain (P21828) increased from 40% to more than 80%, and the peptide coverage of P25 (P04148) also increased by approximately 20%. The increased peptide coverage of ULiD-MS showed that thermal aging was a more extensive degradation, which may provide useful information about the sequence in crystalline regions.

For the global analysis of silk degradation, the total protein intensity and the intensities of the three main proteins (heavy chain, light chain, and p25) at six sampling times (0, 2, 4, 6, 8, and 10 days) were compared. As shown in Figure 7a, the identified total protein intensity dropped to less than half with just 2 days of heat-aging, and a smooth decreasing tendency was observed with prolonged aging time. This decrease in total intensity was essentially caused by a break between the two enzymatic cleavage sites in the protein, as fewer peptides could be identified. Moreover, the ULiD-MS analysis results (Figure 7b) showed a similar degradation trend after the addition of thermally degraded peptides to the protein intensity calculation, only showing some fluctuations in the later stage. The three main proteins detected in all samples are listed in Figure 7c,d. The intensities of all three proteins showed obvious decreasing tendencies, coinciding with the trend of total protein intensity. In particular, the degradation rate of the heavy chain was faster than that of the light chain in LiP-MS analysis, while comparable degradation rates were observed in ULiD-MS analysis. More definitive results are shown in the subsequent relative abundance plots (Figure 8a−c). The proportion of heavy chains was almost unchanged in the early stage of aging but decreased significantly in the later stage in LiP-MS analysis. In contrast, the ULiD-MS result showed that the percentage of heavy chains decreased faster in the early stage. Considering the "GAGAGS" encoding region occupied the vast majority of the nonenzymatic digestion


https://doi.org/10.1021/acsomega.3c02254
ACS Omega 2023, 8, 34410−34419

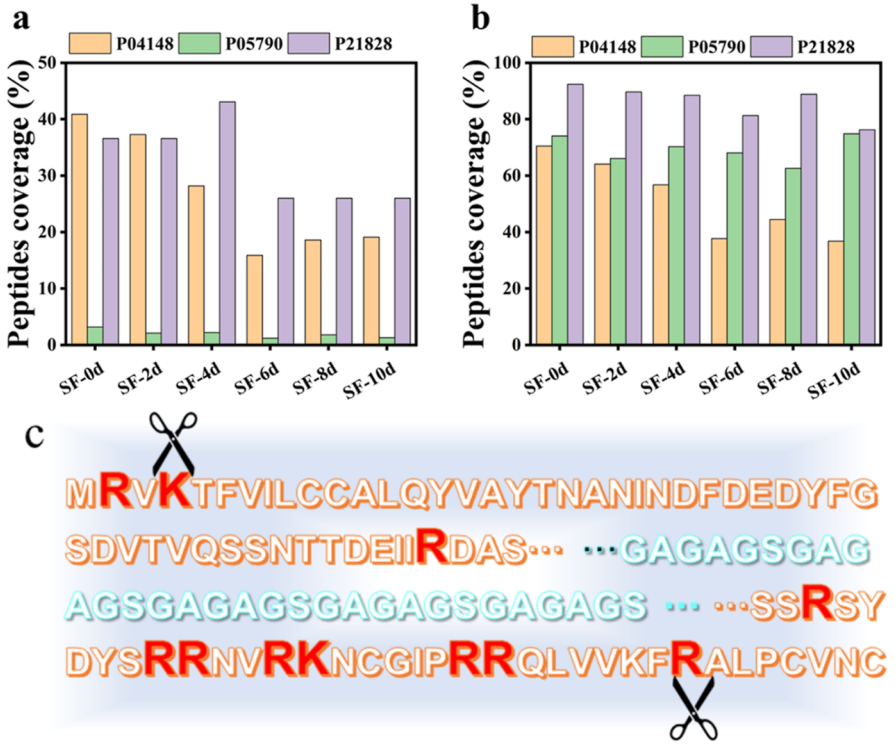


**Figure 6.** Peptide coverage of three protein. (a) LiP-MS analysis; (b) ULiD-MS analysis; (c) schematic diagram of enzymatic digestion by trypsin.

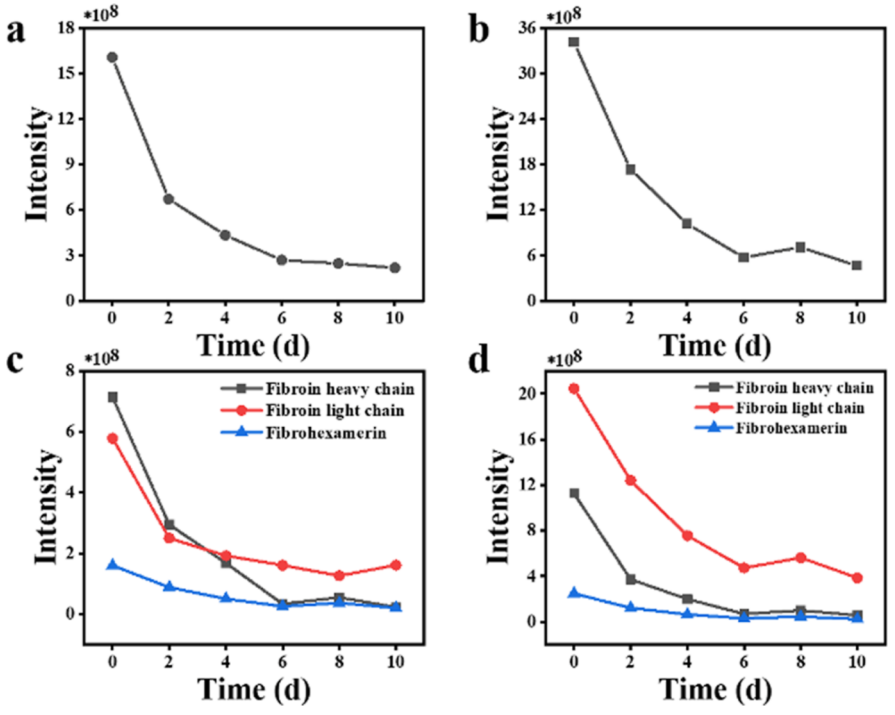


**Figure 7.** (a,b) Total intensity of proteins in silk fibroin and (c,d) the intensity of the three proteins; (a,c) were calculated by LiP-MS analysis, and (b,d) were calculated by ULiD-MS analysis.

region in the heavy chain, it is speculated that the difference may be due to the otherness in the proportion of thermally degraded peptides belonging to the crystallization region in the two proteins.

**Classification Analysis of Peptides in the Fibroin Heavy Chain.** We counted all detected peptides of heavy chains in the ULiD-MS result and divided them into three categories: two-side-digestion peptide (TSD-peptide), one-side-digestion peptide (OSD-peptide), and no-digestion peptide (NOD-peptide). As shown in Figure 10a, few NOD-peptides were detected in the SF-0d sample, indicating that the processes of degumming, weaving, and extraction had damaging effects on the silk. The NOD-peptides overtook TSD-peptides as the main component of the detected peptides as heat-aging proceeded,


https://doi.org/10.1021/acsomega.3c02254
ACS Omega 2023, 8, 34410−34419

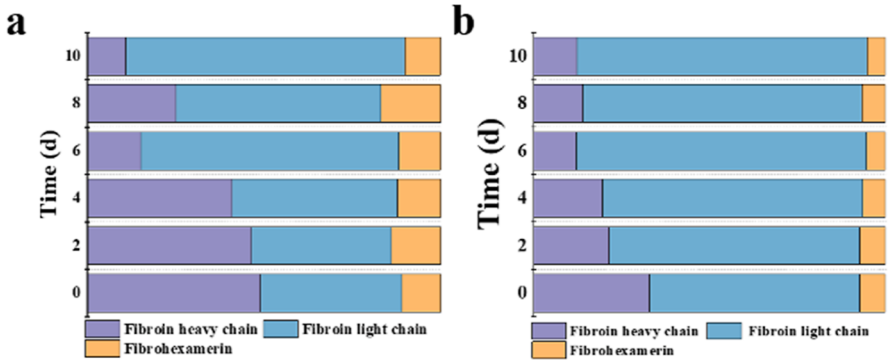


**Figure 8.** Relative abundance of the proteins in silk. (a) LiP-MS analysis and (b) ULiD-MS analysis.

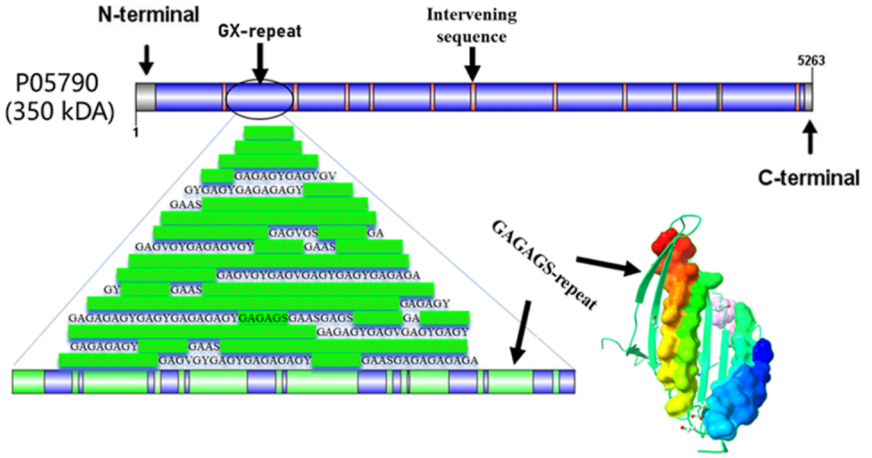


**Figure 9.** Schematic diagram of the structure of the heavy chain.

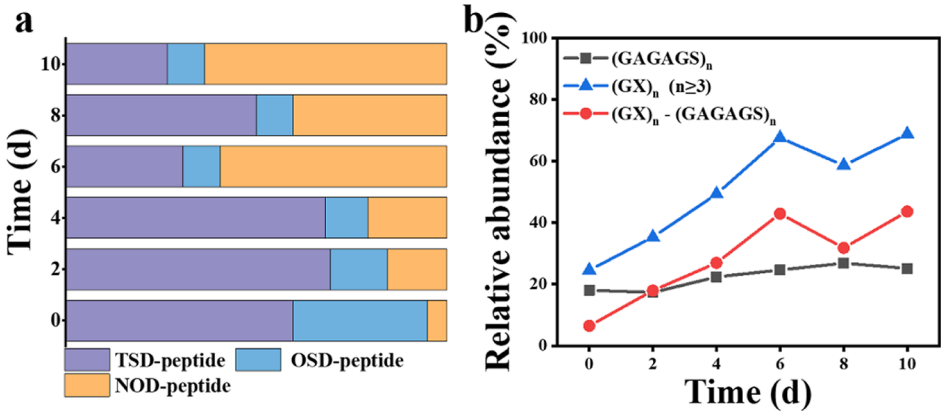


**Figure 10.** (a) Relative abundance of peptides in the fibroin heavy chain (two-side-digestion peptides, one-side-digestion peptides, and no-digestion peptides). (b) Relative abundance of peptides containing $(GAGAGS)_n$ and/or $(GX)_n$ eliminates $(GAGAGS)_n$ segments.

and a large increase in NOD-peptides and a dramatic decrease in TSD-peptides gave direct evidence of heavy chain degradation.

The structural change in silk was one of the main foci of silk aging. As shown in Figure 9, the heavy chain consists of 12 GX-repeat encoding regions separated by 11 random intervening the abundant GX-repeat encoding region (regular region) in the heavy chain was considered to be a major contributor to the crystallinity of silk, especially the highly repetitive "GAGAGS" encoding region (crystalline region). Therefore, direct molecular evidence of the changes in silk crystalline regions can be obtained by monitoring changes in the target peptide groups in the heavy chain. The NOD-peptide, for which both ends of the break were derived from heat-aging degradation, was studied separately and is shown in Figure 10b. As a comparison, the amino acid sequence of the fibroin heavy chain (P05790, downloaded from UniProt-Proteome) was analyzed. Excluding the portion containing the enzymatic cleavage site, the number of amino acids of the $(GX)_n$ ($n \geq 3$) encoding region accounted for 94% of the amino acids in the whole chain, the $(GAGAGS)_n$ ($n \geq 1$) encoding region accounted for 51%, and the completely random region (11 random intervening sequences and part C-terminal and N-terminal) accounted for only 6% (Figure 9). As shown in Figure 10b, the percentage of the random peptide group was above 30% (the theoretical value is approximately


https://doi.org/10.1021/acsomega.3c02254
ACS Omega 2023, 8, 34410−34419

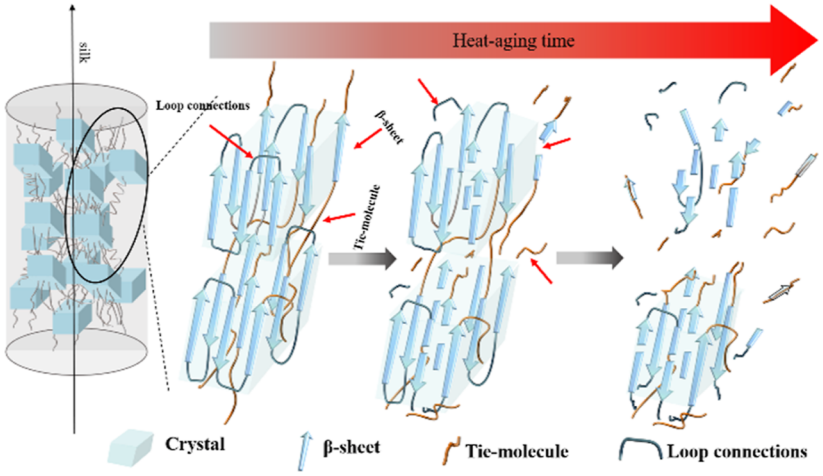


**Figure 11.** Degradation model of thermally aged silk. The amorphous region and crystals are destroyed together. The number of loop connections and tie-molecules between the crystal regions is reduced, and crystal defects appear. Then, the defects continue to increase until the crystal collapses.

6%) throughout the heat-aging process, while the relative abundance of the peptide group containing the $(GAGAGS)_n$ ($n \geq 1$) encoding region was below 28% (the theoretical value is approximately 51%), demonstrating that the crystalline region significantly protected the amino acid sequences being destroyed by heat-aging. However, the percentage of the $(GAGAGS)_n$ ($n \geq 1$) encoding region and the $(GX)_n$ ($n \geq 3$) encoding region slightly increased with the prolongation of the heat-aging time. This seems to indicate that the degradation rate of defective crystals was faster compared to the initial intact crystals, which was more evident in the looser region [$(GX)_n$ ($n \geq 3$) eliminate $(GAGAGS)_n$ ($n \geq 1$)]. The protection of the crystalline region resulted in a lower percentage of thermally degraded peptides in the heavy chain during the early aging stage.

In addition, crystallization inhibited the damage to silk caused by thermal aging, resulting in a lower degradation rate in the crystalline region. In this work, 140 °C was selected as the simulated aging temperature to exclude the influence of water on the properties of silk, and it deviated from the peak range of discrete glass transition temperature (Tg, 150−220 °C).[34] So that the silk fibroin, especially the crystal region, was in an ordered state. Sun's work showed that $(GAGSGA)_2$ short peptide can also form $\beta$-folding,[35] so it might be speculated that after annealing, the thermally degraded peptide in the crystallization zone may attach to the long peptide to maintain the crystal structure, which causes crystallinity to remain unchanged. However, the lowered number of connections of loops and tie-molecules between chain-folding clusters made the thermally aged samples less ductile and thus of poor mechanical performance. As indicated by the intact heavy chain sequence, the long peptides above 50 kDa, which were observed in large numbers in the SF-0d sample, must contain at least one intervening sequence-coding region. Comparatively intact $\beta$-sheet structure and retained random coil conformation were tightly linked, ensuring the strength and toughness of the silk. However, the chemical bonds between crystalline nuclei and other regions were greatly reduced with the prolongation of heat treatment, which led to a constant crystallinity of the silk but a significant decrease in mechanical properties.

**Degradation Model of Heat-Aged Silk Fibroin.** Combining the results presented here, we hypothesized a degradation model to explain the thermal degradation behavior (Figure 11). The random regions act as hinges to connect the crystalline regions, with the random regions providing ductility and the crystalline regions ensuring the strength of the silk. Initially, the thermal degradation is dominated by peptide bond breakage in the amorphous regions, with only minor fractures in the crystalline regions. However, fractures in the amorphous regions can seriously affect the mechanical properties of the silk, whereas fractures in the crystalline regions do not affect crystallinity. As the heat treatment time increases, the long peptides continue to break into short peptides, and the short peptides are completely degraded, while the content of the amorphous regions decreases, and the crystalline regions partially collapse into defective crystals. Although hydrogen bonds maintain the solidity of the crystal, the chemical bonds within the crystal are greatly reduced, resulting in further reduction of the mechanical properties of the silk. Only when the peptide fragments within the crystal nucleus degrade to the point where the crystal shape cannot be maintained will the crystal be transformed into an amorphous one and lose its protective capacity.

## CONCLUSIONS

By the comprehensive analysis of the changes in crystallinity, molecular weight, proteome, and peptidome, we have speculated on the thermal degradation behavior of silk. The degradation behavior of heat-treated silk was microscopically manifested by the reduction in the number of loop connections and tie-molecules between chain-folding clusters as well as the breakage of the crystal nuclei themselves. The changes in crystallinity and peptidome seemed to indicate that the defective $\beta$-fold does not readily convert to the amorphous form. It is worthwhile to expect that ULiD-MS can provide evidence of a more optimized protein extraction process. Meanwhile, due to the protection of silk by the crystalline region, the inverse analysis may allow inferences about the regions to be made about the protein structure.

## ASSOCIATED CONTENT

### Supporting Information

The Supporting Information is available free of charge at https://pubs.acs.org/doi/10.1021/acsomega.3c02254.

Supporting tables and additional results about thermal aging conditions (PDF)



https://doi.org/10.1021/acsomega.3c02254
ACS Omega 2023, 8, 34410−34419

Complementary analysis of proteomics about all protein and peptide identification for both methods (XLSX)

## AUTHOR INFORMATION


### Corresponding Author

**Bing Wang** − *Institute of Textile Conservation, Zhejiang Sci-Tech University, Hangzhou 310018, China;* orcid.org/0000-0002-3499-7828; Phone: +86-571-86843867; Email: wbing388@163.com

### Authors

**Jie Zhou** − *Institute of Textile Conservation, Zhejiang Sci-Tech University, Hangzhou 310018, China*

**Xiong Zhou** − *Institute of Textile Conservation, Zhejiang Sci-Tech University, Hangzhou 310018, China*

**Lindan Pan** − *Institute of Textile Conservation, Zhejiang Sci-Tech University, Hangzhou 310018, China;* orcid.org/0000-0001-9606-265X

**Yefeng Deng** − *Institute of Textile Conservation, Zhejiang Sci-Tech University, Hangzhou 310018, China*

**Hailing Zheng** − *Institute of Textile Conservation, Zhejiang Sci-Tech University, Hangzhou 310018, China; Key Scientific Research Base of Textile Conservation, State Administration for Cultural Heritage, China National Silk Museum, Hangzhou 310002, China;* orcid.org/0000-0003-3257-460X

**Zhiqin Peng** − *Institute of Textile Conservation, Zhejiang Sci-Tech University, Hangzhou 310018, China*

**Junmin Wan** − *Institute of Textile Conservation, Zhejiang Sci-Tech University, Hangzhou 310018, China*

**Yang Zhou** − *Key Scientific Research Base of Textile Conservation, State Administration for Cultural Heritage, China National Silk Museum, Hangzhou 310002, China*

Complete contact information is available at: https://pubs.acs.org/10.1021/acsomega.3c02254


### Author Contributions

The manuscript was written through contributions of all authors. All authors have given approval to the final version of the manuscript.

### Notes

The authors declare no competing financial interest.

## ACKNOWLEDGMENTS

Financial support was provided by the National Key R&D Program of China (2019YFC1520300), the National Natural Science Foundation of China (52273096), and the Special Funds from the Administration of Cultural Heritage of Zhejiang Province (2020012, 2023012).

## REFERENCES


(1) Shimura, K.; Kikuchi, A.; Ohtomo, K.; Katagata, Y.; Hyodo, A. Studies on Silk Fibroin of Bombyx Mori. I. Fractionation of Fibroin Prepared from the Posterior Silk Gland. *J. Biochem.* **1976**, *80* (4), 693−702.

(2) Li, M.-Y.; Zhao, Y.; Tong, T.; Hou, X.-H.; Fang, B.-S.; Wu, S.-Q.; Shen, X.-Y.; Tong, H. Study of the Degradation Mechanism of Chinese Historic Silk (Bombyx Mori) for the Purpose of Conservation. *Polym. Degrad. Stab.* **2013**, *98* (3), 727−735.

(3) Ming, J.; Fan, Z.; Xie, Z.; Jiang, Y.; Zuo, B. A Modified Grey Verhulst Model Method to Predict Ultraviolet Protection Performance of Aging B.Mori Silk Fabric. *Fiber. Polym.* **2013**, *14* (7), 1179−1183.

(4) Zhao, S.; Pan, H.; Liu, Y.; Zeng, Y.; Liu, H.; Yu, W. Silk Fabric Protection Obtained via Chemical Conjugation of Transglutaminase and Silk Fibroin Reinforcement. *Text. Res. J.* **2019**, *89* (21−22), 4581−4594.

(5) Liu, Y.; Peng, Z.; Zhou, Y.; Jia, L.; He, Y.; Yang, D.; Li, H.; Wang, X.; Huang, S.; Zhang, J. Pilot Study on Provenance Tracing of Cocoons via Strontium Isotopes. *Sci. Total Environ.* **2022**, *851*, 157982.

(6) Zhang, W.; Chen, L.; Chen, J.; Wang, L.; Gui, X.; Ran, J.; Xu, G.; Zhao, H.; Zeng, M.; Ji, J.; Qian, L.; Zhou, J.; Ouyang, H.; Zou, X. Silk Fibroin Biomaterial Shows Safe and Effective Wound Healing in Animal Models and a Randomized Controlled Clinical Trial. *Adv. Healthc. Mater.* **2017**, *6* (10), 1700121.

(7) Hu, X.; Shmelev, K.; Sun, L.; Gil, E.-S.; Park, S.-H.; Cebe, P.; Kaplan, D. L. Regulation of Silk Material Structure by Temperature-Controlled Water Vapor Annealing. *Biomacromolecules* **2011**, *12*, 1686−1696.

(8) Brown, J.; Lu, C.-L.; Coburn, J.; Kaplan, D. L. Impact of Silk Biomaterial Structure on Proteolysis. *Acta Biomater.* **2015**, *11*, 212−221.

(9) Chen, R.; Hu, M.; Zheng, H.; Yang, H.; Zhou, L.; Zhou, Y.; Peng, Z.; Hu, Z.; Wang, B. Proteomics and Immunology Provide Insight into the Degradation Mechanism of Historic and Artificially Aged Silk. *Anal. Chem.* **2020**, *92* (3), 2435−2442.

(10) Keten, S.; Xu, Z.; Ihle, B.; Buehler, M. J. Nanoconfinement Controls Stiffness, Strength and Mechanical Toughness of $\beta$-Sheet Crystals in Silk. *Nat. Mater.* **2010**, *9* (4), 359−367.

(11) Tanaka, K.; Kajiyama, N.; Ishikura, K.; Waga, S.; Kikuchi, A.; Ohtomo, K.; Takagi, T.; Mizuno, S. Determination of the Site of Disulfide Linkage between Heavy and Light Chains of Silk Fibroin Produced by Bombyx Mori. *Biochim. Biophys. Acta* **1999**, *1432* (1), 92−103.

(12) Gu, J.; Li, Q.; Chen, B.; Xu, C.; Zheng, H.; Zhou, Y.; Peng, Z.; Hu, Z.; Wang, B. Species Identification of Bombyx Mori and Antheraea Pernyi Silk via Immunology and Proteomics. *Sci. Rep.* **2019**, *9*, 9381.

(13) Tanaka, K.; Inoue, S.; Mizuno, S. Hydrophobic Interaction of P25, Containing Asn-Linked Oligosaccharide Chains, with the H-L Complex of Silk Fibroin Produced by Bombyx Mori. *Insect Biochem. Mol. Biol.* **1999**, *29* (3), 269−276.

(14) Drummy, L. F.; Farmer, B. L.; Naik, R. R. Correlation of the Beta-Sheet Crystal Size in Silk Fibers with the Protein Amino Acid Sequence. *Soft Matter* **2007**, *3* (7), 877−882.

(15) Ha, S.-W.; Gracz, H. S.; Tonelli, A. E.; Hudson, S. M. Structural Study of Irregular Amino Acid Sequences in the Heavy Chain of Bombyx m Ori Silk Fibroin. *Biomacromolecules* **2005**, *6* (5), 2563−2569.

(16) Takahashi, Y.; Gehoh, M.; Yuzuriha, K. Structure Refinement and Diffuse Streak Scattering of Silk (Bombyx Mori). *Int. J. Biol. Macromol.* **1999**, *24* (2−3), 127−138.

(17) Pan, H.; Zhang, Y.; Shao, H.; Hu, X.; Li, X.; Tian, F.; Wang, J. Nanoconfined Crystallites Toughen Artificial Silk. *J. Mater. Chem. B* **2014**, *2* (10), 1408.

(18) Koperska, M. A.; Pawcenis, D.; Bagniuk, J.; Zaitz, M. M.; Missori, M.; Łojewski, T.; Łojewska, J. Degradation Markers of Fibroin in Silk through Infrared Spectroscopy. *Polym. Degrad. Stab.* **2014**, *105*, 185−196.

(19) Fu, C.; Porter, D.; Chen, X.; Vollrath, F.; Shao, Z. Understanding the Mechanical Properties of Antheraea Pernyi Silk-From Primary Structure to Condensed Structure of the Protein. *Adv. Funct. Mater.* **2011**, *21* (4), 729−737.

(20) Zhang, X.; Gong, D.; Gong, Y. Insight into the Orientation Behavior of Thermal-Aged and Historic Silk Fabrics by Polarized FTIR Microspectroscopy. *J. Cult. Herit.* **2019**, *38*, 53−63.

(21) Vinciguerra, R.; Illiano, A.; De Chiaro, A.; Carpentieri, A.; Lluveras-Tenorio, A.; Bonaduce, I.; Marino, G.; Pucci, P.; Amoresano, A.; Birolo, L. Identification of Proteinaceous Binders in Paintings: A Targeted Proteomic Approach for Cultural Heritage. *Microchem. J.* **2019**, *144*, 319−328.

(22) Leo, G.; Cartechini, L.; Pucci, P.; Sgamellotti, A.; Marino, G.; Birolo, L. Proteomic Strategies for the Identification of Proteinaceous Binders in Paintings. *Anal. Bioanal. Chem.* **2009**, *395* (7), 2269−2280.
(23) Schopper, S.; Kahraman, A.; Leuenberger, P.; Feng, Y.; Piazza, I.; Müller, O.; Boersema, P. J.; Picotti, P. Measuring Protein Structural Changes on a Proteome-Wide Scale Using Limited Proteolysis-Coupled Mass Spectrometry. *Nat. Protoc.* **2017**, *12* (11), 2391−2410.
(24) Feng, Y.; De Franceschi, G.; Kahraman, A.; Soste, M.; Melnik, A.; Boersema, P. J.; de Laureto, P. P.; Nikolaev, Y.; Oliveira, A. P.; Picotti, P. Global Analysis of Protein Structural Changes in Complex Proteomes. *Nat. Biotechnol.* **2014**, *32* (10), 1036−1044.
(25) Yoshioka, T.; Takasu, Y.; Sezutsu, H.; Kameda, T. Genome Editing Advances the Structural Study of Silk. *ACS Biomater. Sci. Eng.* **2018**, *4* (3), 832−835.
(26) Wang, F.; Zhang, Y.-Q. Effects of Alkyl Polyglycoside (APG) on Bombyx Mori Silk Degumming and the Mechanical Properties of Silk Fibroin Fibre. *Mater. Sci. Eng. C* **2017**, *74*, 152−158.
(27) Chen, R.; Zhou, L.; Yang, H.; Zheng, H.; Zhou, Y.; Hu, Z.; Wang, B. Degradation Behavior and Immunological Detection of Silk Fibroin Exposure to Enzymes. *Anal. Sci.* **2019**, *35* (11), 1243−1249.
(28) Wang, J.; Guan, J.; Hawkins, N.; Vollrath, F. Analysing the Structure and Glass Transition Behaviour of Silks for Archaeology and Conservation. *J. R. Soc. Interface.* **2018**, *15* (139), 20170883.
(29) Yang, H.; Yang, S.; Kong, J.; Dong, A.; Yu, S. Obtaining Information about Protein Secondary Structures in Aqueous Solution Using Fourier Transform IR Spectroscopy. *Nat. Protoc.* **2015**, *10* (3), 382−396.
(30) Qin, N.; Zhang, S.; Jiang, J.; Corder, S. G.; Qian, Z.; Zhou, Z.; Lee, W.; Liu, K.; Wang, X.; Li, X.; Shi, Z.; Mao, Y.; Bechtel, H. A.; Martin, M. C.; Xia, X.; Marelli, B.; Kaplan, D. L.; Omenetto, F. G.; Liu, M.; Tao, T. H. Nanoscale Probing of Electron-Regulated Structural Transitions in Silk Proteins by near-Field IR Imaging and Nano-Spectroscopy. *Nat. Commun.* **2016**, *7* (1), 13079.
(31) Carissimi, G.; Baronio, C. M.; Montalbán, M. G.; Víllora, G.; Barth, A. On the Secondary Structure of Silk Fibroin Nanoparticles Obtained Using Ionic Liquids: An Infrared Spectroscopy Study. *Polymers* **2020**, *12* (6), 1294.
(32) Li, M.; Tao, W.; Lu, S.; Kuga, S. Compliant Film of Regenerated Antheraea Pernyi Silk Fibroin by Chemical Crosslinking. *Int. J. Biol. Macromol.* **2003**, *32* (3−5), 159−163.
(33) Gillet, L. C.; Leitner, A.; Aebersold, R. Mass Spectrometry Applied to Bottom-Up Proteomics: Entering the High-Throughput Era for Hypothesis Testing. *Annual Rev. Anal. Chem.* **2016**, *9* (1), 449−472.
(34) Guan, J.; Porter, D.; Vollrath, F. Thermally Induced Changes in Dynamic Mechanical Properties of Native Silks. *Biomacromolecules* **2013**, *14* (3), 930−937.
(35) Sun, H.; Marelli, B. Polypeptide Templating for Designer Hierarchical Materials. *Nat. Commun.* **2020**, *11* (1), 351.


https://doi.org/10.1021/acsomega.3c02254
*ACS Omega* 2023, 8, 34410−34419